

Strain, size and composition of InAs Quantum Sticks, *embedded* in InP, by means of Grazing Incidence X-ray Anomalous Diffraction

A. Letoublon¹, V. Favre-Nicolin^{1,2}, H. Renevier^{1,2}

M.G. Proietti³, C. Monat⁴, M. Gendry⁴

O. Marty⁵, C. Priester⁶

¹*Commissariat à l'Energie Atomique, Département de Recherche Fondamentale sur la Matière Condensée, SP2M/NRS, 17 rue des martyrs, 38054 Grenoble Cedex 9, France.*

²*Université Joseph Fourier, BP 53, F-38041, Grenoble Cedex 9, France.*

³*Departamento de Física de la Materia Condensada, Instituto de Ciencia de Materiales de Aragón, CSIC-Universidad de Zaragoza - c. Pedro Cerbuna 12, 50009 Zaragoza, Spain.*

⁴*LEOM, UMR-CNRS 5512, Ecole Centrale de Lyon, 69134 Ecully, France.*

⁵*LENAC, Université Lyon I, 69621 Villeurbanne, France. and*

⁶*Institut d'Electronique, de Microélectronique et de Nanotechnologie, dep. ISEN, 59652 Villeneuve d'Ascq, France.**

(Dated: 22/09/03, submitted)

We have used x-ray anomalous diffraction to extract the x-ray structure factor of InAs quantum stick-like islands, *embedded* in InP. The average height of the quantum sticks (Qs), as deduced from the width of the structure factor profile is 2.54nm. The InAs out of plane deformation, relative to InP, is equal to 6.1%. Diffraction Anomalous Fine Structure provides a clear evidence of pure InAs Qs. Finite Difference Method calculations reproduce well the diffraction data, and give the strain along the growth direction. Chemical mixing at interfaces is at most of 1ML

PACS : 68.65.La 61.10.Nz

Band structure gives the optical and electronic properties of materials. It can be strongly modified by reducing the size of semiconductor material down to a length scale comparable

*Electronic address: Hubert.Renevier@cea.fr

to the effective wave-length of the carriers, i.e. in the order of several nanometers, leading to discrete energy levels [1]. Much study has been done on InAs quantum structures such as Quantum Wires (QWr) and Quantum Dots (QD). With an emission wavelength which can be around $1.55\mu\text{m}$, such nanostructures are of interest for the next generation of integrated circuits (telecommunication relevant range of $1.3\text{-}1.6\mu\text{m}$). The nano-objects we are interested in are grown by Molecular Beam Epitaxy (MBE) and obtained via the Stranski-Krastanov growth. The lattice mismatch $\frac{a_{\text{InAs}}-a_{\text{InP}}}{a_{\text{InP}}}$ is about 3.2%. Recent studies [2] have shown that a strong stress anisotropy appears during the growth deposition leading to a higher stress along the $[110]$ direction than along the $[\bar{1}\bar{1}0]$. The stress is released first in the $[110]$ direction leading to the QWr formation. To be suitable for devices, the nanostructures are encapsulated with InP or embedded in a superlattice, they must be homogeneous in size, shape and composition, to provide well defined emission wavelengths. The knowledge of strain field, chemical gradients, chemical mixing at the interface, is of great importance to understand the growth dynamics as well as the electronic and optical properties of the nanostructures.

We report on an x-ray study of InAs stick-like islands embedded in InP with 10 nm thick capping layer. These samples are obtained by optimisation of the MBE growth parameters to minimize the As/P exchange and reduce the height dispersion of the InAs islands [3, 4]. The width of photoluminescence (PL) peaks reveals a very good height homogeneity [5], as confirmed by Transmission Electron Microscopy (TEM) measurements. The InAs islands obtained with a nominal deposition thickness of 4ML are 50 to 200nm long along the $[\bar{1}\bar{1}0]$ direction (1a). As shown by cross-section TEM image the QDs exhibit a truncated triangle side shape with typical width of 22.5 ± 0.12 nm and homogeneous height, of 2.4 nm (figure 1b).

In the present paper we show that the structure factor of embedded nanostructures can be directly determined by means of grazing incidence anomalous x-ray diffraction, allowing to recover the average height and strain of the QDs, to determine their composition and check the As/P exchange. As a matter of fact, strain of buried nanostructures is not directly related to composition (Vegard's law), but it also depends on size, morphology, and cap layer thickness. Then, tuning the x-ray energy near an absorption edge of atoms that belong to the nanostructures is a way to modify their scattering power and to enhance the chemical sensitivity of diffraction. Previous studies have shown the interest of using

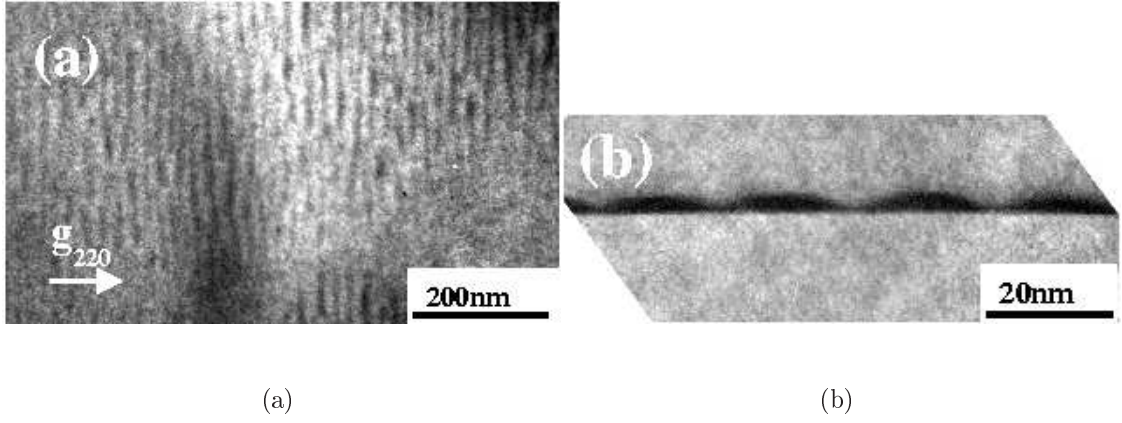


Figure 1: Transmission Electron Microscopy images of InAs QDs embedded in InP (a) plane view, (b) cross section ; one can clearly see the truncated triangle shape

anomalous diffraction to determine strain and composition in InAs QWs grown on InP [6] or large Ge dots grown on Si [7, 8]. We report on a general method that takes advantage of the full capability of anomalous diffraction [9] and can be applied to the very interesting and challenging case of *small size embedded* nanostructures, the x-ray scattering yield of which is overwhelmed by the dominant matrix contribution, whatever the momentum transfer is.

Grazing incidence anomalous diffraction intensity, can be written in the frame of the Distorted Wave Born Approximation [10, 11] :

$$I(\vec{Q}, E) \propto \|T_i(\alpha_i, E)\|^2 \|F_T(\vec{Q})\|^2 \left[(\cos(\varphi_T - \varphi_A) + \beta f'_{As})^2 + (\sin(\varphi_T - \varphi_A) + \beta f''_{As})^2 \right] \quad (1)$$

where F_T is a complex structure factor of phase φ_T which includes the overall contribution of non anomalous atoms and the Thomson scattering of all anomalous atoms, $\beta = \frac{\|F_A\|}{f_{As}^0 \|F_T\|}$ where F_A is a complex structure factor of phase φ_A which includes the Thomson scattering of all anomalous atoms (i.e. As atoms). $\|T_i(\alpha_i, E)\|^2$ is the incidence transmittivity, and α_i is the incidence angle that is close to the critical angle α_c . In the following, the exit angle is much larger than the critical angle, then the exit transmittivity $\|T_f(\alpha_f, E)\|^2 = 1$ and the scattering length ($\approx 100nm$) is much larger than the epilayer thickness. The As scattering factor writes $f_{As} = f_{As}^0 + f'_{As} + i f''_{As}$, where f'_{As} and f''_{As} are the real and imaginary resonant scattering of As atoms. Equation 1 shows that diffraction measurements at various energies (at least 3) at the As K-edge, allow to recover a quantity that is proportional to the F_T modulus, the β ratio and the phase difference $\Delta\varphi = \varphi_T - \varphi_A$. The knowledge of $\|F_A\|$ and

$\Delta\varphi$ readily gives information about the average size and strain of the nanostructures and chemical mixing at interface.

Grazing incidence Anomalous diffraction at the As K-edge (11.867 KeV) was performed at the French Collaborative Research Group beamlines BM32 and BM2 at the European Synchrotron Radiation Facility, using a Si(111) double crystal monochromator to select energies and mirrors to reject harmonics. Grazing incidence was used to minimize the substrate contribution. We recorded the scattering intensity in the vicinity of the (442) substrate reflection, at several energies across the As K-edge. We chose a weak reflection ($h+k+l=4n+2$) for which the anomalous diffraction contrast is maximum; it lies in the mirror plane defined by the [110] and [001] directions to benefit from symmetry in the reciprocal space. Figure 2 shows the diffraction intensity map recorded at 11.840 keV and at a grazing incidence angle equal to the critical angle ($\alpha_i = \alpha_c = 0.2^\circ$) to maximize the diffraction intensity. For that reflection the exit angle α_f is about 20° . A large amount of information can be drawn from such a map : the spreading of scattering in the [110] direction is due to both short range correlation and lattice strain in the corresponding direction in the real space ([110]) whereas, in the [001] direction it is due to the sharp strain evolution. Figure 2 shows correlation satellites on both sides of the (442) (S1 and S2) their positions relative to the substrate peak give a qualitative estimation of the mean correlation distance between the wires. We find a value of $20.7nm$, that is in agreement with the TEM.

The markable result in this map, is the clear asymmetry of the S1 and S2 satellites ; S1 exhibits a broad and twin feature along the [001] direction, with a sharp splitting at $l=2$, whereas S2 is a single feature centered approximately at $l=2$. S1 corresponds to regions stretched along the [110] direction (tensile strain), i.e. to InAs sticks and InP regions located below and above the sticks. S2, instead, corresponds to InP which is compressed in between of the sticks. Indeed, anomalous diffraction measurements at the As K-edge show no significant intensity variations of satellite S2 as a function of the energy, confirming that the InP contribution is the dominant one. Furthermore, these measurements also show firstly, that the transmittivity corrections can be neglected, secondly, that the wetting layer, if it exists, must be very thin, at most one ML. Cutoff fringes are clearly observed in the l direction around the substrate Bragg peak position and give the total thickness of both the InAs QDs and the InP capping, that is equal to $11 \pm 0.3nm$.

We performed l -scans ($h=k=3.98$) across the satellite S1, at nine different energies close

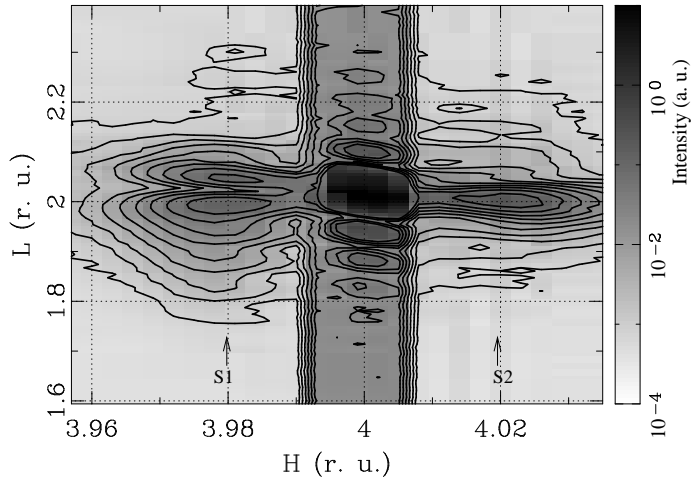


Figure 2: Experimental diffraction map around the weak (442) reflection recorded at 11.840 KeV in grazing incidence geometry ($\alpha_i = \alpha_c = 0.2^\circ$, $\alpha_f \simeq 20^\circ$). S1 and S2 are correlation satellites due to the stick short range periodicity.

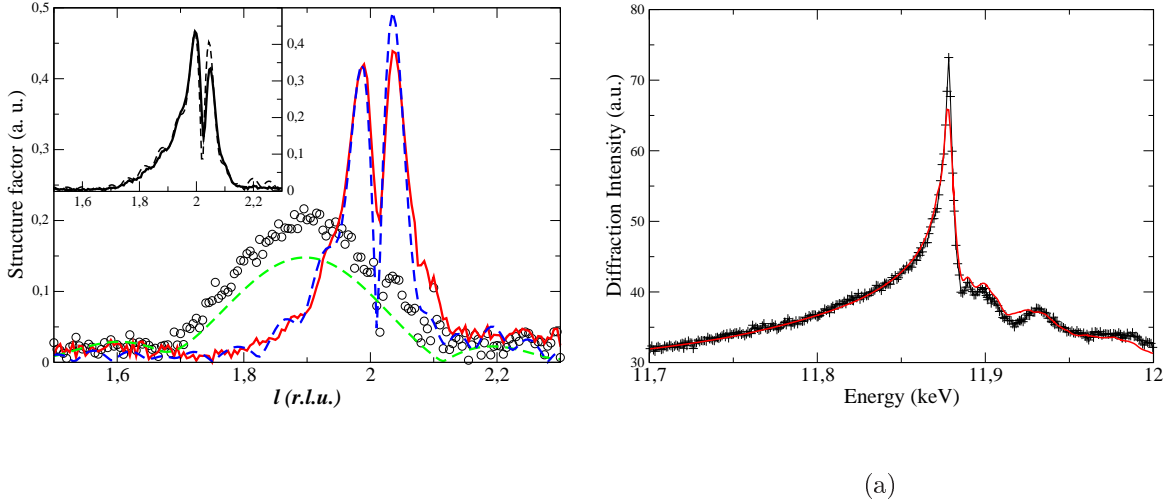


Figure 3: (a) Experimental F_T (solid line) and F_A (ooo) modulus as a function of the reciprocal lattice unit l at $h=k=3.98$ (across the satellite S1). F_A is the structure factor that corresponds to all anomalous atoms, i.e. As atoms only. Also shown are best simulation curves (dashed line) obtained with a FDM model made of pure InAs Qs with a truncated triangle side profile. Inset shows the experimental (solid line) and simulated (dashed line) square root of the diffraction intensity at 11.867keV ; at this energy, anomalous diffraction is maximized. (b) GI- DAFS spectrum recorded, at the As K-edge, at the maximum of the F_A profile ($l=1.9$) and the best fit curve obtained with pure InAs structure (solid line).

to the As K-edge including those corresponding to the minimum of f'_{As} and the white line of f''_{As} . A weak fluorescence background was subtracted and the data were normalized to \mathbf{l} -scans across the satellite S2, measured at the same energies. Then $F_A(\vec{Q})$, $F_T(\vec{Q})$ and $\Delta\varphi(\vec{Q})$ were extracted by fitting equation 1 to the energy dependent experimental intensities.

Figure 3a) shows the experimental modulus of $F_A(\vec{Q})$, $F_T(\vec{Q})$. The QSs height average value ($\langle H \rangle$) can be estimated from the Full Width at Half Maximum (FWHM) of F_A , $\langle H \rangle = \frac{c_{InP}}{0.9 \times (\Delta F_A)_{FWHM}} = 2.54nm$, that is very near of the value measured with TEM. In order to determine the QSrs composition and the local strain accomodation, Grazing Incidence Diffraction Anomalous Fine Structure spectrum was measured at the maximum of F_A ($\mathbf{h}=\mathbf{k}=3.98$ and $\mathbf{l}=1.9$) at the As K-edge. Figure 3b) shows the experimental DAFS spectrum and the simulation calculated with the crystallographic structure of $InAs_{1-x}P_x$ and the anomalous scattering factors f'_{As} and f''_{As} of bulk InAs. A scale factor, the detector efficiency as a function of the energy and the As occupation factor $(1-x)$ were refined. The best fit curve, shown on figure 3b) corresponds to a value of $(1-x)$ equal to 1.03, i.e. the QSs composition is *pure* InAs. GIDAFS oscillations, in the energy range above the edge, will give also direct information on the local composition and on strain accomodation inside the sticks. Detailed analysis of these oscillations will be reported elsewhere.

Finite Difference Method simulations were performed to map the strain produced by InAs QSs embedded in InP and compare its Fourier Transform to experimental diffraction intensity maps. We assumed a coherent growth of InAs on InP (supported by the lack of dislocations seen in TEM micrography). We performed Finite Difference Method calculations [12], in a 2D periodic frame, in the plane determined by the [110] and [001] crystal axis, i.e. the wires have infinite length along $[1\bar{1}0]$ and a periodic structure along the [110]. The QSs length is finite and rather short (50-200nm), meaning 2D calculations slightly overestimate the strain, the relaxation along [110] being not permitted. We chose an FDM cell with a size of $\frac{\sqrt{2}a}{4} \times \frac{a}{4}$. Then, atoms are placed inside the crystallographic cell according to Cubic Face Centered Zinc-blende structure, taking into account elastic deformation. Starting from atomic positions, diffraction intensity is then calculated using the Distorted Wave Born Approximation [10]. No structural disorder has been taken into account. The P and In anomalous scattering factors were obtained from theoretical values, whereas experimental values for As in bulk InAs were used.

Figures 4a) and 4b), show the deformation maps with respect to InP lattice parameter,

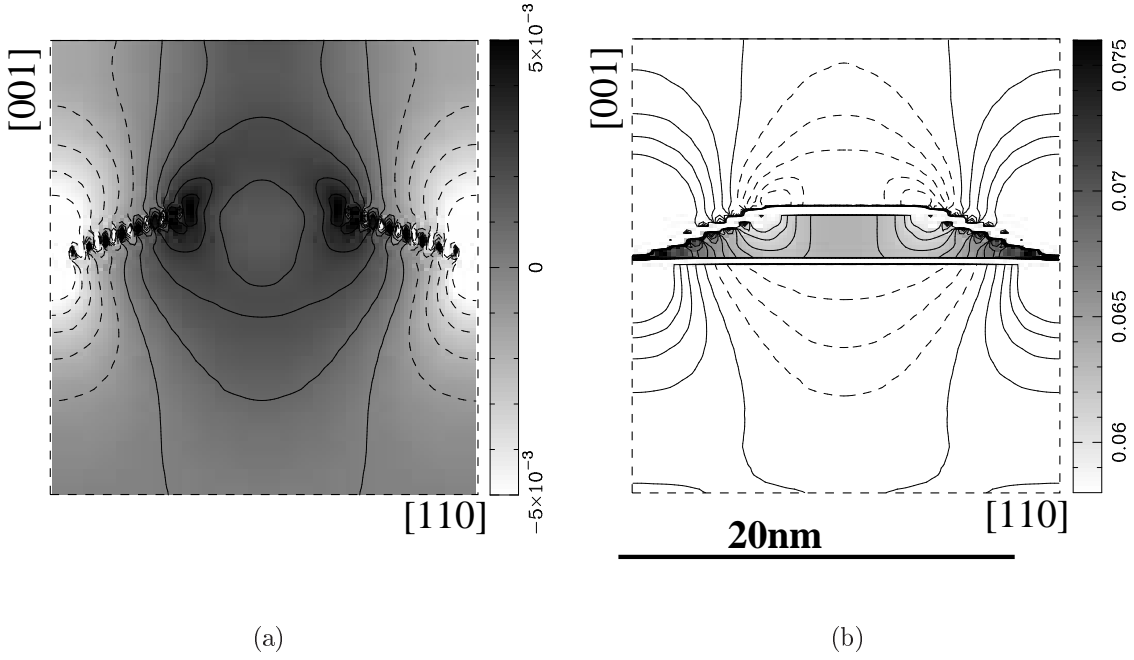


Figure 4: FDM simulations of (a) $\varepsilon_{xx} = \frac{a_{ij} - a_{InP}}{a_{InP}}$ and (b) $\varepsilon_{zz} = \frac{c_{ij} - c_{InP}}{c_{InP}}$, where a_{ij} and c_{ij} are the parameters of cell (i,j). The strain is relative to bulk InP cell parameter, it is not the relative displacement. The ε_{zz} clearly show the morphology of InAs QWrs. Solid and dashed lines represent positive and negative contour strain, respectively, starting at $-5 \cdot 10^{-3}$ and spaced by .001. Ten additional ε_{zz} contours are shown inside the wire starting at 0.06. The solid line on top represents the sample surface.

obtained with a model of embedded InAs QWrs as deduced from TEM images (fig. 1b), that well reproduces the diffraction data. The QWrs side shape is a truncated triangle as shown by TEM. The total thickness of the QWrs and the capping is equal to 11nm, as reported above. Figure 4b) shows a map of deformations along the [001] direction (ε_{zz}), which emphasizes the morphology of the wires. Indeed the wires are compressed along [110] (with partial relaxation shown in fig. 4a), thus expanded along [001]. This explains the sharp contrast of lattice strain shown in figure 4b) (ε_{zz}). Figure 4a) shows the relative strain ε_{xx} along [110], here it is impossible to disentangle InAs from InP regions under and on the top of the wires, since the in-plane lattice strain is continuous at the interface. On figure 3a) are shown the best calculated curves of F_A and F_T , obtained by optimizing the height and width of the wires, as well as As/P intermixing at the InAs/InP interface. The splitting of F_T is well reproduced by the simulation and is due to a scattering phase shift between InP

cells above and below the wires. The overall wire thickness and width are found to be 9 MLs and 22nm, respectively. The simulated ratio $\beta = \frac{\|F_A\|}{f_{As}\|F_T\|}$ at the maximum of F_A is equal to 0.113, i.e close to the experimental value of 0.124 deduced from the GI-DAFS spectrum (figure 3b). Note that FDM simulation well reproduces the relative positions of F_A and F_T , with a strain ε_{zz} of about 6.3% in the inner part of the wire. For comparison, the strain of a pseudomorphic InAs thin film grown on InP, as foreseen by the elastic theory, is 6.7%. The $\varepsilon_{zz} = \frac{c-c_{InP}}{c_{InP}} = \frac{l_{InP}-l_{FA}}{l_{FA}}$ value, deduced directly from the reciprocal lattice position l_{FA} of the maximum of F_A (fig. 3a) is equal to $6.1\pm 0.25\%$, i.e., within the uncertainty, equal to the value simulated with FDM. Regarding composition, our FDM simulations show that the QDs inner part is pure InAs. The experimental curves (F_A and F_T) are compatible with a weak As/P intermixing at the InP interface, that would spread over one ML. Indeed, improving the signal-to-noise ratio together with a 2D data treatment, would allow to fully exploit the technique sensitivity to map the composition at the ML scale.

In conclusion, we have shown that anomalous diffraction can be used to extract the structure factor of small size InAs nanostructures *embedded* in InP matrix. This study is a first step towards a 2D and 3D analysis of anomalous diffraction maps and Grazing Incidence DAFS data to recover the strain, size, shape and composition of *embedded* nanostructures.

We are very grateful to F. Né, J.S Micha, S. Arnaud, B. Caillot and J.F. Bézar for help during the experiments at the beamlines BM32 and BM2 at the ESRF. M.G.P and H.R. Acknowledge the support of Egide and Aciones Integradas Programmes (grant ref. HF2002-78) of the French and Spanish ministries of Research and Education.

-
- [1] D. Bimberg, M. Grundman, and N. Ledensov, *Quantum Dots heterostructures* (Wiley, Chis-
teter, 1999).
 - [2] L. González, J. M. García, R. García, J. Martínez-Pastor, and C. Ballesteros, Appl. Phys.
Lett. **76**, 1104 (2000).
 - [3] C. Monat, M. Gendry, J. Brault, M. Besland, P. Regreny, G. Hollinger, B. Salem, J. Olivares,
G. Bremond, and O. Marty, in *Proceedings of the 14th IPRM, IEEE Stockholm* (2002), p. 565.
 - [4] M. Gendry, C. Monat, J. Brault, P. Regreny, G. Hollinger, B. Salem, G. Guillot, T. Benyattou,
C. Bru-Chevallier, G. Bremond, et al., J. Appl. Phys. (2003), submitted.

- [5] B. Salem, T. Benyattou, G. Guillot, C. Bru-Chevallier, G. Bremond, C. Monat, G. Hollinger, and M. Gendry, Phys. Rev. B **66**, 193305 (2002).
- [6] S. Grenier, M. Proietti, H. Renevier, L. Gonzalez, J. Garcia, and J. Garcia, Europhys. Lett. **57**, 499 (2002).
- [7] R. Magalhaes-Panagio, G. Medeiros-Riberio, A. Malachias, S. Kycia, T. Kamins, and R. Stan, Phys. Rev. B **66**, 245312 (2002).
- [8] T. Schüllli, J. Stangl, Z. Zhong, R. Lechner, M. Sztucki, T. Metzger, and G. Bauer, Phys. Rev. Lett. **90**, 66105 (2003).
- [9] J. Hodeau, V. Favre-Nicolin, S. Bos, H. Renevier, J. Lorenzo, and J. Bézar, Chem. Rev. **101**, 1843 (2001).
- [10] H. Dosch, *Critical Phenomena at Surfaces and Interfaces* (Springer Verlag, 1992).
- [11] M. Proietti, H. Renevier, J. Hodeau, J. Garcia, J. Bézar, and P. Wolfers, Phys. Rev. B **59**, 5479 (1999).
- [12] Y. Niquet, C. Priester, C. Gourgon, and H. Mariette, Phys. Rev. B **57**, 14850 (1998).